ARL-TR-10192 ● SEP 2025

Condensed-Phase Property Estimates for Ethyl Nitrate Derived from Atomistic Equilibrium Molecular Dynamics Simulations

by Jeffrey D. Veals, Joshua L. Lansford, Chiung-Chu Chen, and Christopher P. Stone

NOTICES

Disclaimers

The findings in this report are not to be construed as an official Department of the Army position unless so designated by other authorized documents.

Citation of manufacturer's or trade names does not constitute an official endorsement or approval of the use thereof.

Destroy this report when it is no longer needed. Do not return it to the originator.

ARL-TR-10192 ● SEP 2025

Condensed-Phase Property Estimates for Ethyl Nitrate Derived from Atomistic Equilibrium Molecular Dynamics Simulations

Jeffrey D. Veals, Joshua L. Lansford, Chiung-Chu Chen, and Christopher P. Stone
DEVCOM Army Research Laboratory

REPORT DOCUMENTATION PAGE

1. REPORT DATE	2. REPORT TYPE	3. DATES COVERED	
		START DATE	END DATE
September 2025	Technical Report	1 March 2025	30 June 2025

4. TITLE AND SUBTITLE
Condensed-Phase Property Estimates for Ethyl Nitrate Derived from Atomistic Equilibrium Molecular Dynamics Simulations

5a. CONTRACT NUMBER	5b. GRANT NUMBER	5c. PROGRAM ELEMENT NUMBER
5d. PROJECT NUMBER	**5e. TASK NUMBER**	**5f. WORK UNIT NUMBER**

6. AUTHOR(S)
Jeffrey D. Veals, Joshua L. Lansford, Chiung-Chu Chen, and Christopher P. Stone

7. PERFORMING ORGANIZATION NAME(S) AND ADDRESS(ES)
DEVCOM Army Research Laboratory
ATTN: FCDD-RLA-WC
Aberdeen Proving Ground, MD 21005

8. PERFORMING ORGANIZATION REPORT NUMBER
ARL-TR-10192

9. SPONSORING/MONITORING AGENCY NAME(S) AND ADDRESS(ES)	10. SPONSOR/MONITOR'S ACRONYM(S)	11. SPONSOR/MONITOR'S REPORT NUMBER(S)

12. DISTRIBUTION/AVAILABILITY STATEMENT
DISTRIBUTION STATEMENT A. Approved for public release: distribution unlimited.

13. SUPPLEMENTARY NOTES
ORCIDs: Jeffrey D. Veals, 0000-0002-8238-345X; Joshua L. Lansford, 0000-0001-8245-3190; Chiung-Chu Chen, 0000-0002-8666-9949; Christopher P. Stone, 0000-0002-9621-5334

14. ABSTRACT
This study contributes to a broader program to develop ML-based methods that reduce the time and cost to expand the ARL's detailed chemical kinetics library. To support future combustion modeling, we model properties of ethyl nitrate (EN), a key surrogate for more complex nitrate esters. We perform atomistic equilibrium molecular dynamics simulations with the AMBER force field under a constant number of particles, pressure, and temperature conditions. We estimate key condensed-phase properties over temperatures ranging from 193 to 600 K. These properties include densities, enthalpies of vaporization, and self-diffusion coefficients. Our findings, particularly the diffusion coefficients, serve as a basis for computing rate coefficients for elementary condensed-phase reactions, thereby advancing our understanding of EN's condensed-phase reaction behavior. The enthalpy-of-vaporization estimates in this work, combined with gas-phase enthalpy-of-formation estimates from previous work, result in condensed-phase enthalpy-of-formation estimates ranging from −7.2 to −0.4 kJ/mol of measured values. Using the diffusivity data, we derive a hole-free volume function ($P_{HFV}(T)$), indicating that condensed-phase reaction rates are likely to be significantly lower than gas-phase rates at temperatures relevant to combustion (e.g., less than 5% at 500 K). These results inform ongoing development of multiphase modeling, specifically liquid- and gas-phase EN combustion.

15. SUBJECT TERMS
Weapons Sciences, propulsion, chemical kinetics, pyrolysis, molecular dynamics, self-diffusion, viscosity, free volume theory, ML, machine learning, D-MPNN, directed-message passing neural network

16. SECURITY CLASSIFICATION OF:			17. LIMITATION OF ABSTRACT	18. NUMBER OF PAGES
a. REPORT	b. ABSTRACT	C. THIS PAGE		
UNCLASSIFIED	UNCLASSIFIED	UNCLASSIFIED	UU	25

19a. NAME OF RESPONSIBLE PERSON	19b. PHONE NUMBER *(Include area code)*
Jeffrey D. Veals	(520) 942-1877

STANDARD FORM 298 (REV. 5/2020)
Prescribed by ANSI Std. Z39.18

Contents

List of Figures

List of Tables

Acknowledgments

This research was supported by the U.S. Army Combat Capabilities Development Command Army Research Laboratory's Machine Learning to Accelerate Detailed Finite-Rate Chemical Kinetics Mechanism Creation for Continuum-Level Modeling of Energetic Material Decomposition and Combustion mission program. Molecular dynamics simulations used DoD High Performance Computing Modernization Program resources. We thank Dr. Michael J. McQuaid (ARL) for his valuable guidance and recommendation for this study.

1. Introduction

Developing accurate chemical kinetics mechanisms remains a significant challenge for modeling the decomposition and combustion of energetic materials (EMs). This report describes efforts to predict thermodynamic and transport properties of condensed-phase EMs, including key properties needed for the detailed modeling of EM pyrolysis and combustion. This research is part of a larger program at the U.S. Army Combat Capabilities Development Command (DEVCOM) Army Research Laboratory (ARL) to accelerate the development of comprehensive chemical kinetics mechanisms for use in modeling propellant combustion and propulsion systems. A key aim of this program is to employ ML methods to accelerate mechanism creation by learning from existing data and focusing computational effort on the most important chemical reactions. To support these goals, we incorporate theoretical models linking gas-phase behavior to condensed-phase dynamics. Techniques such as pyrolysis gas chromatography-mass spectrometry[1] and opposed flow flame experiments[2] provide data used to validate model predictions, ultimately improving simulations of condensed-phase pyrolysis and advancing our understanding of propellant processes. This effort builds on our team's prior work.[3,4]

We use a free volume theory framework[5] with the function [P_{HFV}], defined in the equation under Section 3.5, representing the hole-free volume probability, to translate gas-phase rate coefficients into condensed-phase equivalents. Effective P_{HFV} parameterization relies on temperature-dependent viscosity or self-diffusion coefficient estimates (see extensive background in McQuaid et al.[3]). Although accurately measured dynamic viscosities are optimal, self-diffusion coefficients can be efficiently estimated in lieu of costly measurements using atomistic molecular dynamics (MD) simulations. Previous work on nitroglycerin[6] demonstrated a strong correlation between decomposition rate increases and changes in condensed-phase free volume, challenging the autocatalytic mechanism proposed by Waring and Krastins.[7] The present work extends this methodology to the parameterization of P_{HFV} for ethyl nitrate (EN).

EN has long been studied for its physical properties[8,9] and combustion behavior.[10–17] Its relative simplicity as a primary nitrate ester[18] makes it a valuable model for understanding more complex nitrate esters like isopropyl nitrate (iPN), n-butyl nitrate, and nitroglycerin.[6,19–21]

ARL researchers[22] previously developed detailed gas-phase chemical kinetics mechanisms for EN and methyl nitrate, which were validated by comparison with measured burning rates (i.e., regression rates). That work, using computational

chemistry and transition state theory, provided key thermochemical parameters and reaction rates.

Building on these prior efforts and to support physics-based modeling applications, we employed equilibrium MD (EMD) modeling to characterize key condensed-phase properties of EN as a function of temperature. These include mass density, enthalpy of vaporization, and molecular transport rates (self-diffusion and viscosity). We integrated the gas-phase enthalpy-of-formation estimates from the previous work[22] with our current results to determine condensed-phase enthalpy-of-formation. Critically, we also estimated a hole-free volume probability function and a condensed-phase enthalpy-of-formation for use as inputs to ARL's two-phase EM combustion model (i.e., liquid-gas). We anticipate that this model will improve chemical kinetics development and validation against experimental results, ultimately informing strategies for controlling the combustion of more complex nitrate esters and other propellant ingredients. In this report, we present the details of our EMD study and the resulting condensed-phase properties.

2. Computational Methods

The EMD protocol used in this work follows the same methodology established in our prior investigations of 1,5,9-decatriene (DTE) and myrcene (MYR),[9,23] hydroxyl-terminated 6-ethenyl-2,8,12,16-octadecetetraene (EODT) oligomers [HO-(EODT)n-OH],[24] and iPN.[25] EMD simulations were performed using the LAMMPS MD framework.[26] For forcefield selection, we followed our iPN approach[25] by employing the Class I general AMBER force field (GAFF) with parameters previously validated for nitrate esters plasticizers,[27] rather than the Class II force fields (PCFF and COMPASS) used in earlier studies.[28-30]

2.1 Simulation Setup and Protocols

The methods and protocols used throughout this study are outlined in Figure 1. Initial topology files for a single EN molecule were generated with the ACPYPE Server,* which leverages the Antechamber program within AmberTools. Starting from the input xyz coordinate file, the software program generated the initial structure and assigned atomic charges, which were then manually adjusted to achieve a net charge of zero. The resulting structure and atom types are shown in Figure 2, and the modified AM1-BCC charges are detailed in Table 1.

* ACPYPE Server, https://bio2byte.be/acpype/

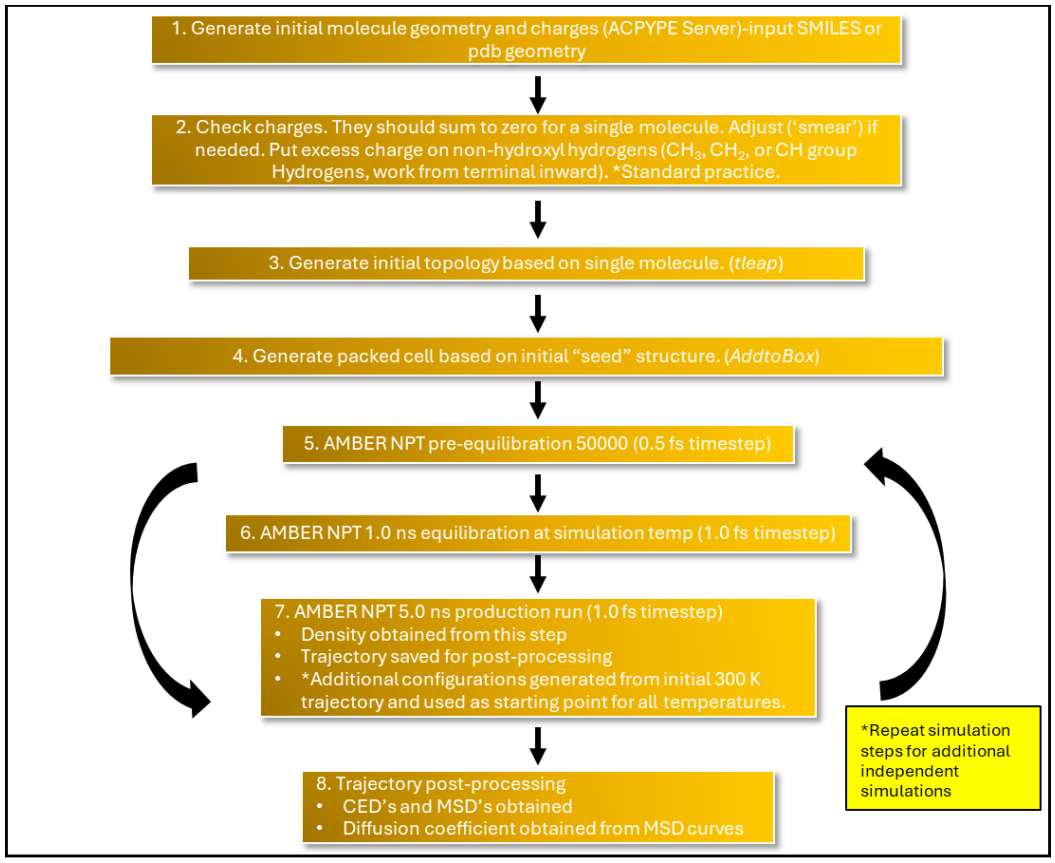

Figure 1. Methodology for topology creation, system setup, and simulation protocol used to estimate physical properties.

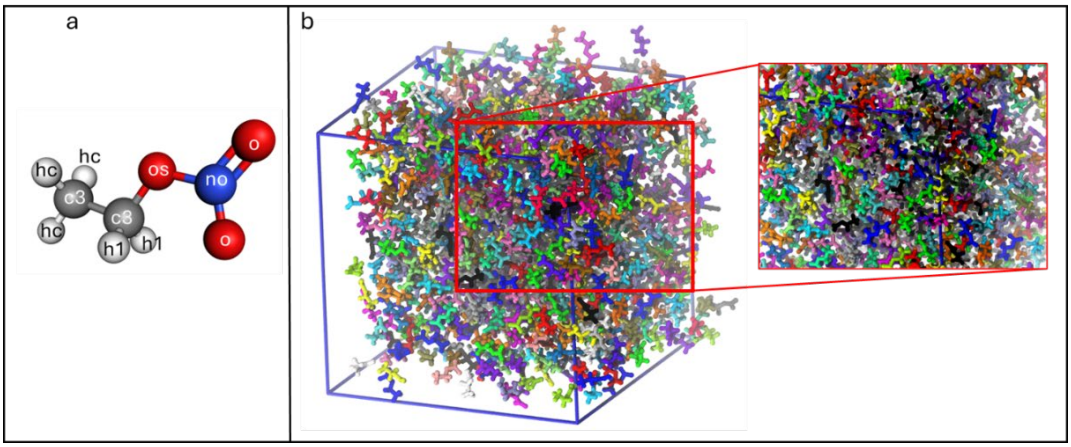

Figure 2. Molecular representation of EN for atomistic simulations. (a) EN molecular structure with GAFF atom types indicated. (b) Snapshot of a simulation cell containing 900 EN molecules at 300 K, where each molecule is represented by a different color for clarity.

Table 1. Atom type and partial charges of each atom of EN.[a]

Atom type	AM1-BCC charge
c3 ($-CH_3$)	−0.1361
c3 ($-CH_2$)	0.1334
os	−0.348
no	0.3752
o	−0.185
o	−0.185
hc	0.0600332
hc	0.0600332
hc	0.0600332
h1	0.0827002
h1	0.0827002

[a] In-house parameters are used for nonbond, bonds, and angles involving c3, os, no, and o atom types. Amber defaults are used for nonbond, bond, and angle parameters involving the remaining atom types hc and h1.

Next, The AMBERTools *tleap* program was used to generate a topology file for a single molecule, and the resultant bond and angle parameters were adjusted to match those previously determined.[30] Simulation boxes were then created and populated with molecules using the AMBERTools *AddToBox* program, using an algorithm to maintain a minimum separation distance of 3 Å between intermolecular atoms.

Energy minimization and a short simulation using constant number of particles, pressure, and temperature (NPT) conditions were performed to reduce excessive repulsive interatomic interactions. A system of 10,000 atoms was needed to converge properties of interest in our previous work with the similarly sized iPN molecule.[25] Therefore, we conducted simulations using a system of 9900 atoms (i.e., 900 molecules).

Atomic coordinates, atom types, and topology information from the pre-equilibrated cells were used to create starting configurations for all temperatures. Each cell underwent a three-stage equilibration process before production simulations. Electrostatic interactions were calculated using the particle-particle particle-mesh implementation of Ewald summation in LAMMPS, and the van der Waals interactions were modeled with 12-6 Lennard–Jones functions. Constant pressure and temperature were maintained using a Nosé–Hoover barostat and thermostat, respectively.

The equilibration protocol began with a 0.05-ns NPT run at the target temperature, followed by a 1-ns run at the target temperature, using a 1-fs time step. A 5-ns NPT production run was then performed with a 1-fs time step. Thermostat and barostat relaxation times were 0.1 and 1 ps, respectively, and coordinates were saved every 10 ps.

Ten arbitrary frames from the initial production run (spaced approximately 0.5 ns apart) were re-equilibrated and used to launch new production runs to produce a wider range of independent trajectories. These subsequent runs were conducted at 15 temperatures over the range of 190–600 K. For these respective runs, a temperature ramp to 600 K was performed, and then the system was cooled to the respective production run temperature. The upper production run temperature limit was set based on Zeldovich's[31] observation of rapid evaporation in superheated liquids, and this is consistent with the boiling points of DTE and MYR (approximately 440 K), iPN (approximately 375 K), and EN (approximately 360 K) reported in previous studies. We anticipate that results at higher temperatures would provide minimal additional information.

2.2 Self-Diffusion Coefficients

One widely used method for calculating diffusion coefficients (D) from MD simulations, as discussed by Maginn et al.,[32] is based on the "Einstein" equation and relies on the calculation of the mean square deviation (MSD) of particle positions. The expression is shown by Equation 1:

$$D = \frac{1}{2d_\alpha N} \lim_{t \to \infty} \frac{\langle |\boldsymbol{r}(t) - \boldsymbol{r}(0)|^2 \rangle}{\mathrm{d}t}, \quad (1)$$

where d_α is the number of dimensions, N is the number of particles, and $\langle |\boldsymbol{r}(t) - \boldsymbol{r}(0)|^2 \rangle$ is the mean square deviation (MSD) of the particles' positions $[\boldsymbol{r}(t)]$ at a given time (t) compared with their starting positions $\boldsymbol{r}(0)$. Because Equation 1 computes D values from MSDs as "t→ ∞," it is assumed that longer simulations will produce more accurate results. Maginn et al.[32] advised focusing on the "diffusive regime," a linear portion of the MSD versus time plot, which can be identified through a slope of approximately 1 in a plot of ln(MSD) against ln(t). Following the protocol that we used in our study of DTE and MYR (and most recently iPN), we ran simulations with production runs of 5 ns. As stated previously, this length was adequate for these smaller molecules to find durations (t_d) in which MSD versus t plots for $0.25t_d \leq t \leq 0.50t_d$ ($t_0 \leq t \leq t_{max}$) were reasonably linear (Equation 2):

$$\mathrm{MSD}(t) = m(t - 0.25t_d)^{n'=1} + b', \quad (2)$$

where m and b were constants and t_d = 5 ns. We obtained the value of n' (Equation 3) by fitting

$$\ln(\mathrm{MSD}(t) - b') = \ln(m) + n' \ln(t - 0.25t_d) \quad (3)$$

to interval data. Substituting m into Equation 4, with d_α= 3, yields

$$D = \frac{m}{6N}. \quad (4)$$

2.3 Thermodynamic Parameters

The condensed-phase enthalpy-of-formation for liquid EN ($\Delta_f H_c(T)$) was obtained by subtracting estimates of the EMD-based vaporization enthalpy ($\Delta H_v(T)$) from gas-phase enthalpy-of-formation estimates ($\Delta_f H_g(T)$) obtained through quantum mechanical and electronic structure modeling (QM-ESM).

The EMD simulations provided cohesive energies (E_{coh}), defined as the average intermolecular nonbonded energy per mole,[33] which were then used to approximate the vaporization enthalpy (see Equation 5):

$$\Delta H_v(T) \approx E_{coh}(T) + RT, \quad (5)$$

with R representing the universal gas constant. The $\Delta_f H_g(T)$ values were based on established thermodynamic properties for EN, determined in Chen and McQuaid's[22] previous studies to develop a detailed chemical kinetics mechanism for EN.

3. Results and Discussion

3.1 Density Estimates

Table 2 presents $\rho(T)$ estimates for EN in the range of 190–600 K. As found previously for other nitrate ester systems,[30] AMBER-based estimates for these small nitrate esters are quite reasonable. In this study, the estimated value of 1.173 g/cm^3 is 0.065 g/cm^3 greater (5.5%) than the experimental value of 1.1084 g/cm^3 at 293 K. Such agreement is reassuring and supports using the force field parameter set in a generalized way for nitrate esters because EN was not explicitly involved in fitting these parameters. Over the full temperature range of 190.15–600 K, the density decreases by 53% from 1.303 to 0.607 g/cm³. Limiting the upper temperature to the experimental boiling point of EN (approximately 360 K[*])[18] results in a 16% decrease in density. Assessing the reliability of EMD-based results at temperatures above 298 K is difficult to do with the limited amount of elevated temperature measured property data for EN.

[*]Experimental boiling point of EN is approximately 361 K.

Table 2. AMBER and measured $\rho(T)$ values for EN at 1 atm.

T (K)	ρ (g/cm^3)	Measured
190.15	1.303	. . .
200.15	1.291	. . .
225.15	1.259	. . .
250.15	1.227	. . .
273.15	1.198	. . .
293.15	1.173	1.10[a]
300.15	1.163	. . .
325.15	1.132	. . .
350.15	1.099	. . .
375.15	1.066	. . .
400.15	1.03	. . .
450.15	0.958	. . .
500.15	0.876	. . .
550.15	0.775	. . .
600.15	0.607	. . .

[a]Measured density[34]

3.2 Enthalpy-of-Vaporization Estimates

Table 3 presents $\Delta H_v(T)$ estimates for EN between 190 and 600 K. The AMBER $\Delta H_v(T)$ estimates show excellent agreement with the limited available experimental data, which is consistent with previous findings for small nitrate esters.[4] Specifically, the AMBER estimates near 288 K fall within the range of measured values, reinforcing confidence in the model's accuracy near standard temperature and pressure.

Similar to our recent report for iPN,[25] we also employed an ML directed-message passing neural network (D-MPNN) model that was previously developed for predicting the vapor pressures of EMs[35] to evaluate EN's enthalpy-of-vaporization between 190 and 600 K. The aim of this assessment was to determine the ML model's potential for future applications of estimating the enthalpy-of-vaporization of energetic molecules of interest to us, offering a faster and more cost-effective alternative to MD simulations, particularly when MD force field parameters are unavailable.

Table 3. Estimated (AMBER, D-MPNN) and measured $\Delta H_v(T)$ for EN at 1 atm.

T (K)	ΔH_{vap} (kJ/mol)		
	AMBER	D-MPNN	Measured
190.15	45.1	. . .	. . .
200.15	44.4	. . .	. . .
225.15	42.8	. . .	. . .
250.15	41.3	35.16	. . .
273.15	39.9	. . .	. . .
288	. . .	. . .	37[a], 37.3[b]
293.15	38.8	35.16	. . .
298	. . .	. . .	36.28[c]
300.15	38.4	35.16	. . .
325.15	37.0	. . .	. . .
350.15	35.6	. . .	. . .
375.15	34.3	. . .	. . .
400.15	33.0	. . .	. . .
450.15	30.5	. . .	. . .
500.15	27.8	. . .	. . .
550.15	24.9	. . .	. . .
600.15	20.6	. . .	. . .

[a]At 288 K.[36]
[b]At 288 K.[8]
[c]At 298 K.[8]

The D-MPNN ΔH_v estimate was smaller than the AMBER-based estimate. At 298 K, the ML-based value is within 1 kcal/mol of the measured value.

3.3 Condensed-Phase Enthalpy-of-Formation Estimates

We found that $\Delta_f H_g(T)$ estimates (in kJ/mol) for EN in the range of 190–600 K were well represented by the formula shown by Equation 6,

$$\Delta_f H_g^{EN}(T) = -182.93 + 5.779\text{x}10^{-2}T + 7.748x10^{-5}T^2\,, \qquad (6)$$

and AMBER-based $\Delta H_v(T)$ estimates for it (in kJ/mol) were well represented by the formula shown by Equation 7,

$$\Delta_f H_v^{EN}(T) = 54.99 - 5.309x10^{-2}T - 4.817x10^{-6}T^2. \qquad (7)$$

Subtracting Equation 7 from Equation 6 yielded the result shown by Equation 8:

$$\Delta_f H_c^{EN}(T) = -237.93 + 1.109x10^{-1}T + 8.230x10^{-5}T^2\,. \qquad (8)$$

Equation 8 predicts a liquid-phase enthalpy-of-formation of −197.6 kJ/mol at 298 K, consistent with available data. An independent estimate using the D-MPNN model's predicted enthalpy-of-vaporization yields −193.6 kJ/mol at the same temperature. Our computational estimates deviate from previously reported experimental values (−190.4 ± 1.0 and −191 ± 3.0 kJ/mol) by −7.2 to −3.6 kJ/mol

(AMBER-based) and −3.2 to −0.4 kJ/mol (D-MPNN-based), demonstrating close agreement within experimental uncertainty (Table 4).

Table 4. Estimated (AMBER, D-MPNN) and measured condensed-phase enthalpy of formation of EN at 1 atm.

$\Delta_f H_c^{EN}(298\ \mathrm{K})$[a]	Source
−197.6	Current EMD
−193.6	Current D-MPNN
−190.4 ± 1.0	Fairbrother et al.[37]
−191.0 ± 3.0	Gray and Smith[9]

[a] Units in kJ/mol.

3.4 Self-Diffusion Coefficient Estimates

Figure 3 shows mean-squared displacement versus time plots for EN at 190 and 600 K. Diffusivity (D) was computed from MSD(t) values between 1.25 and 2.50 ns, obtained from 5-ns simulations. The plots show variability between independent simulations (run 0–9), especially at longer times.

Table 5 presents the [MSD (5 ns)]$^{1/2}$, $D(T)$, and $ln[D(\mathrm{cm}^2/\mathrm{s})]$ estimates for EN. [MSD (5 ns)]$^{1/2}$ values show the travel distance for each *tracked* atom type during the simulations. These values confirm that the 5-ns simulation durations were adequate for accurate *D(T)* estimates across the temperature range of interest (i.e., the tracked atoms have diffused a sufficient distance away from their starting location over the 5-ns simulation for all temperatures).

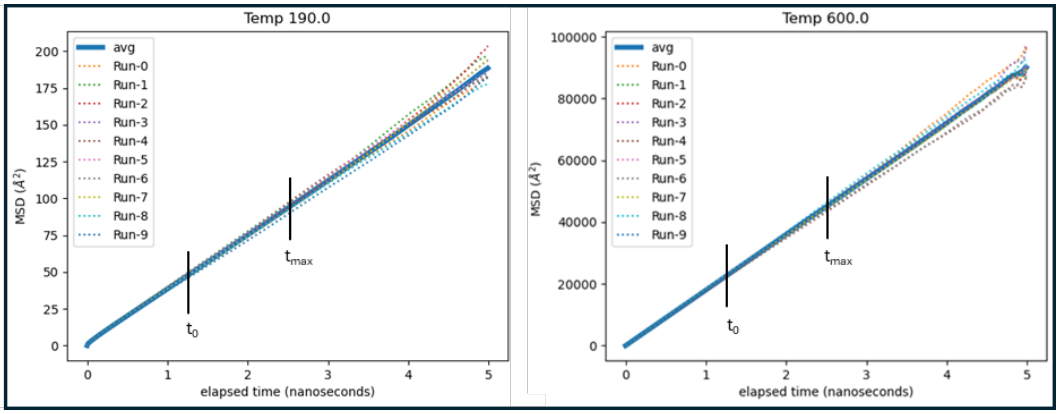

Figure 3. AMBER-based MSD vs. *t* trajectories for EN at 190 and 600 K.

Table 5. AMBER-based [MSD(5 ns)]$^{1/2}$, D, and $ln(D)$ estimates for EN at 1 atm.

T (K)	[MSD(5 ns)]$^{1/2}$ (Å)	D (cm^2/s)	$ln(D)$	Estimated η[a] (cP)	Measured η (cP)
190	13.7	6.13E-07	−14.3	1.303	. . .
200	18.5	1.13E-06	−13.7	1.291	. . .
225	31.3	3.24E-06	−12.6	1.259	. . .
250	43.6	6.30E-06	−12	1.227	. . .
273	55.4	1.01E-05	−11.5	1.198	. . .
289	. . .	. . .	. . .	. . .	0.56[b]
293	65.8	1.46E-05	−11.1	1.173	0.66,[c] 0.87[d]
300	69.8	1.63E-05	−11	1.163	. . .
325	82.5	2.28E-05	−10.7	1.132	. . .
350	95.4	3.04E-05	−10.4	1.099	. . .
375	108.4	3.91E-05	−10.1	1.066	. . .
400	122.2	5.01E-05	−9.9	1.03	. . .
450	151.8	7.60E-05	−9.5	0.958	. . .
500	183.1	1.13E-04	−9.1	0.876	. . .
550	227.9	1.72E-04	−8.7	0.775	. . .
600	300.0	3.01E-04	−8.1	0.607	. . .

[a] Estimated from calculated diffusion coefficients using the expression $\eta(T) = \left(\frac{1}{2\pi}\right)\left(\frac{kT}{D(T)}\right)\left(\frac{N_A}{V}\right)^{\frac{1}{3}}$.

[b] Measured viscosity of methyl nitrate at 289 K.[38]

[c] Measured viscosity of iPN at 289 K.[39]

[d] Measured viscosity of n-butyl nitrate at 289 K.[18]

Limited experimental transport data are available for EN, although data exists for similar-sized nitrate esters. Abbott[39] reported a viscosity of 0.66 cP at 293 K for the slightly larger iPN, whereas methyl nitrate and n-butyl nitrate have measured viscosities of 0.56 (at 289 K) and 0.87 cP (at 293 K), respectively.

Viscosity estimates were obtained from our AMBER-based MD diffusion coefficients using the equation $\eta(T) = \left(\frac{1}{2\pi}\right)\left(\frac{kT}{D(T)}\right)\left(\frac{N_A}{\bar{V}}\right)^{\frac{1}{3}}$, where k is Boltzmann's constant, N_A is Avogadro's number, T is absolute temperature in kelvin, D is the diffusion coefficient, and $\bar{V}$ is molar volume. This yielded an MD-based estimate of 1.173 cP at 293 K, which is approximately 0.3 cP higher than that of n-butyl nitrate. Obtaining precise predictions with a general force field not specifically parameterized for this property is challenging, and assessing temperature trends requires measured data across a range of temperatures. Nevertheless, our MD-predicted value is within 1 order of magnitude of the available experimental data for related nitrate esters, which suggests that our modeling approach reasonably captures the system's physics. Any remaining discrepancies likely stem from limitations in the force field functional form and/or parameterization, consistent with our previous findings.[25]

3.5 Probability Function Parameterizations

McQuaid et al.[3] previously proposed a framework for estimating rate coefficients for elementary condensed-phase reactions, centered around the P_{HFV} function. P_{HFV} evaluates the likelihood of reactive sites being adjacent to a free-volume hole large enough to facilitate a reaction while preventing diffusive reversal. Based on free volume theory, we established a relationship between P_{HFV} and the diffusion constant, $D(T)$:

$$D(T) = AP_{HFV}(T) = Aexp\left(\frac{-B}{T-T_0}\right). \quad (9)$$

To estimate P_{HFV}, we fit Equation 9 to AMBER-based $ln[D]$ versus temperature data for EN. Figure 4 shows the resulting curve, along with the fit of $ln(A) - [B/(T-T_0)]$ to the data, and corresponding curve for iPN. As observed previously for liquid nitrate esters[3] $\exp[-B/(T - T_0)]$ reasonably represents the temperature dependence of D. The magnitudes of B and T_0 for EN are somewhat smaller than those for iPN, but they are larger than those from previous nitrate ester work.[3] Overall, these values remain within the same order of magnitude, providing some confidence in the results.

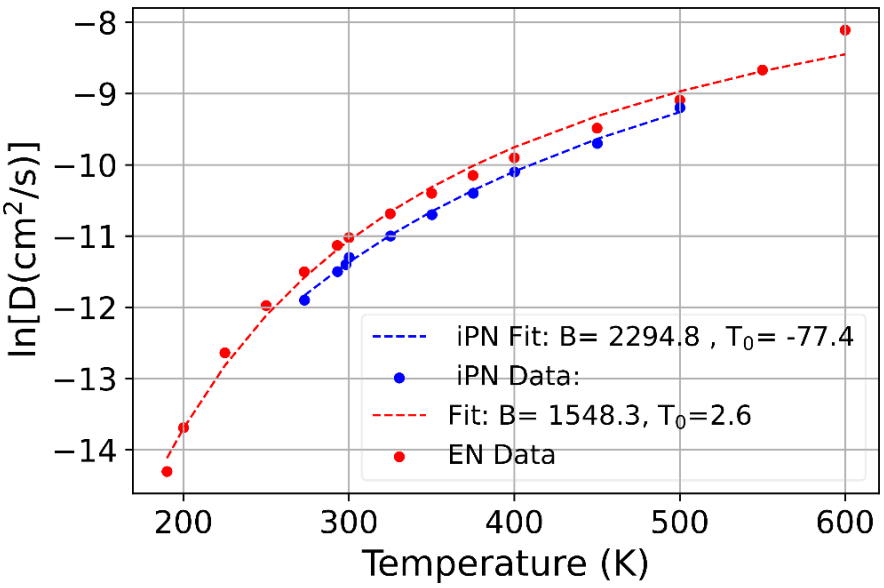

Figure 4. ***ln*[*D*(*T*)] estimates for EN compared with previous data for iPN.**

Our previous work demonstrated that force field choice can significantly impact P_{HFV} predictions. Further investigation is needed to assess the potential influence of the AMBER force field on our current predictions. Nevertheless, based on these estimates, EN condensed-phase rates are predicted to be less than 5% of their gas-phase counterparts at 500 K (Figure 5). A value comparable to that predicted for iPN and those of DTE and MYR, respectively. These results require corroboration.

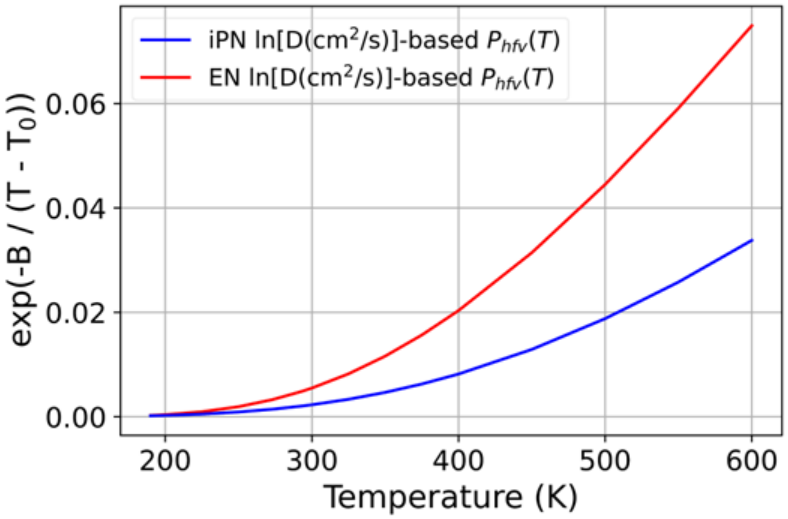

Figure 5. P_{HFV} **estimates for EN compared with previous results for iPN.**

4. Summary and Conclusion

As part of an effort to develop and apply ML methods for accelerating the creation of detailed chemical kinetics mechanisms for combustion modeling, EMD simulations were performed to estimate the density, enthalpy-of-vaporization, and self-diffusivity of condensed-phase EN. Comparison with available experimental measurements confirms the utility of these estimates and the methodology proposed in this report.

We also presented calculated condensed-phase enthalpy-of-formation values by combining enthalpy-of-vaporization estimates (AMBER EMD simulations or D-MPNN ML model) with QM-ESM-based gas-phase enthalpy-of-formation estimates. These calculated values appeared reasonable. In addition, the diffusivity estimates were used to parameterize a $P_{HFV}(T)$ function, suggesting that elementary condensed-phase reaction rates will be less than 5% of their gas-phase counterparts at temperatures up to 500 K. However, this estimate requires corroboration. Our work will contribute to future combustion modeling of EN and validation of a novel two-phase model against available experimental data.

5. References

1. Pesce-Rodriguez R, McQuaid M. Toward validating a framework for modeling high-throughput analytical techniques employed for energetic material screening. Part 2. Desorption/pyrolysis-gas-chromatography/mass spectrometry (D/P-GC/MS) results for beta-myrcene. DEVCOM Army Research Laboratory (US); 2024 Jan. Report No.: ARL-TN-1192.

2. McQuaid MJ, Chen C-C, Stone CP, Veals JD. On modeling the pyrolysis of hydroxyl-terminated polybutadiene (HTPB) type R45M at temperatures in the range 465–600 °C. DEVCOM Army Research Laboratory (US); 2023 May. Report No.: ARL-TR-9681.

3. McQuaid MJ, Veals JD, Yeh I-C, Chen C-C. The development of detailed finite-rate chemical kinetics mechanisms for modeling decomposition in condensed phases. Part 2. The parameterization of free volume theory for liquid nitrate esters. Proceedings of the 50th JANNAF Combustion Subcommittee Meeting; 2020 Dec 7–17; Virtual.

4. Veals JD, I-C Yeh, Chen C-C, Andzelm JW, McQuaid MJ. Establishing and parameterizing rate coefficient functions for steps in the decomposition of nitrate esters in condensed phases: progress in developing a practical approach. Proceedings of the 41st JANNAF Propellant and Explosives Development and Characterization Subcommittee Meeting; 2018 Dec 10–13; Vancouver, WA.

5. Cohen MH, Turnbull D. Molecular transport in liquids and glasses. J Chem Phys. 1959;31(5):1164–1169.

6. McQuaid MJ, Chen C-C, Veals JD, Yeh I-C. Detailed finite-rate chemical kinetics-based modeling of the decomposition of nitroglycerin in systems comprising liquid and gas phases. Proceedings of the 43rd JANNAF Propellant and Explosives Development and Characterization Subcommittee Meeting; 2021 Dec 6–16; Virtual.

7. Waring CE, Krastins G. Kinetics and mechanism of the thermal decomposition of nitroglycerin. J Phys Chem. 1970;74(5):999–1006.

8. Gray P, Pratt MWT. 414. The latent heats of vaporization of the alkyl nitrates. J Chem Soc. (Resumed). 1957:2163–2168.

9. Gray P, Smith PL. Low-temperature calorimetry and the thermodynamic properties of ethyl nitrate. J Chem Soc. (Resumed). 1954:769–773.

10. Fifer RA. High temperature pyrolysis of methyl (and ethyl) nitrate. Symposium (International) on Combustion. 1979;17(1):587–599.

11. Levy JB. The thermal decomposition of nitrate esters. I. Ethyl nitrate1. J Am Chem Soc. 1954;76(12):3254–3257.

12. Levy JB. The thermal decomposition of nitrate esters. II. The effect of additives on the thermal decomposition of ethyl nitrate1. J Am Chem Soc. 1954;76(14):3790–3793.

13. Batt L, Milne RT, McCulloch RD. The gas-phase pyrolysis of alkyl nitrites. IV. Ethyl nitrite. Int J Chem Kinet. 1977;9(4):567–587.

14. Houser TJ, Lee BMH. Pyrolysis kinetics of ethyl nitrate. J Phys Chem. 1967;71(11):3422–3426.

15. Pollard FH, Marshall HSB, Pedler AE. The thermal decomposition of ethyl nitrate. Trans Faraday Soc. 1956;52(0):59–68.

16. Steinberger R, Orlick CA, Schaaf VP. Burning rates of deuterated nitrate esters. J Am Chem Soc. 1955;77(18):4748–4750.

17. Hildenbrand DL, Whittaker AG, Euston CB. Burning rate studies. I. Measurement of the temperature distribution in burning liquid strands. J Phys Chem. 1954;58(12):1130–1133.

18. Urbanski T. Chemistry and technology of explosives. 1964.

19. Morin J, Bedjanian Y. Kinetic and mechanistic study of the thermal decomposition of ethyl nitrate. Int J Chem Kinet. 2017;49(5):354–362.

20. Zaslonko IS, Smirnov VN, Tereza AM. High-temperature decomposition of methyl, ethyl, and isopropyl nitrates in shock waves. Kinet Catal. 1993;34(4):531–538.

21. Schwind RA, Goldsmith CF. Experimental study of linear burning rates of liquid isopropyl nitrate. Combust Flame. 2023;257:112591.

22. Chen C-C, McQuaid MJ. A detailed, gas-phase, finite-rate chemical kinetics mechanism for modeling the combustion of methyl and ethyl nitrate. Proceedings of the 60th JANNAF Propulsion Meeting; 2013 Apr 29–May 2. Colorado Springs, CO.

23. Veals JD, Chen C-C, Yeh I-C, Stone, CS, McQuaid MJ. Condensed-phase property estimates for 1,5,9-decatriene and myrcene derived from atomistic molecular dynamics simulations. DEVCOM Army Research Laboratory (US); 2023 June. Report No.: ARL-TN-1162.

24. Veals JD et al. Property estimates for hydroxyl-terminated polybutadiene (HTPB) type R45M derived from atomistic molecular dynamics simulations.

DEVCOM Army Research Laboratory (US); 2023 June. Report No.: ARL-TR-9714.

25. Veals JD, Lansford JL, Chen C-C, Stone CP, Cornell R. Condensed-phase property estimates for isopropyl nitrate derived from atomistic equilibrium molecular dynamics simulations. Proceedings of the 45th JANNAF Propellant and Explosives Development and Characterization Meeting; 2024 Dec 9−13; Charlotte, NC.

26. Plimpton S. Fast parallel algorithms for short-range molecular dynamics. J Comput Phys. 1995;117(1):1–19.

27. Yeh I-C et al. Detailed representations for condensed phase nitrate ester reaction chemistry: Part 1. Force field parameterization and validation for methyl nitrate. 2017.

28. Sun H. Ab initio calculations and force field development for computer simulation of polysilanes. Macromolecules. 1995;28(3):701–712.

29. Bunte SW, Sun H. Molecular modeling of energetic materials: The parameterization and validation of nitrate esters in the COMPASS force field. J Phys Chem. B. 2000;104(11):2477–2489.

30. McQuaid MJ, Sun H, Rigby D. Development and validation of COMPASS force field parameters for molecules with aliphatic azide chains. J Comput Chem. 2004;25(1):61–71.

31. Zeldovich JB. On the theory of formation of a new phase, cavitation. J Exp Theor Phys. 1942;12:525.

32. Maginn EJ et al. Best practices for computing transport properties 1. Self-diffusivity and viscosity from equilibrium molecular dynamics. LiveCoMS. 2018;1(1):6324.

33. Barton AF. CRC handbook of solubility parameters and other cohesion parameters. 2017; Routledge.

34. Meyer R, Köhler J, Homburg A. Explosives. 2016; John Wiley & Sons.

35. Lansford JL, Jensen KF, Barnes BC. Physics-informed transfer learning for out-of-sample vapor pressure predictions. Propell Explos Pyrot. 2023;48(4):e202200265.

36. Stephenson RM, Malanowski S. Handbook of the thermodynamics of organic compounds. Elsevier; 1987.

37. Fairbrother DM, Skinner HA, Evans FW. The heats of combustion of organic compounds of nitrogen. Part 1. Ethyl, n-propyl, and isopropyl nitrates. Trans Faraday Soc. 1957;53(0):779–783.

38. Gol'binder A, Goryachev V. Pulsatory combustion of liquid explosives thickened with dissolved polymers. Russ J Phys Chem. 35:889–891.

39. Abbott A. The monopropellant isopropyl nitrate - its characteristics and uses, and possible future applications. Proceedings of the AIAA/SAE/ASME 16th Joint Propulsion Conference. 1980 June 30–July 2; Hartford, CT.

List of Symbols, Abbreviations, and Acronyms

ARL	Army Research Laboratory
atm	atmosphere
COMPASS	condensed-phase optimized molecular potentials for atomistic simulation studies
DEVCOM	U.S. Army Combat Capabilities Development Command
D-MPNN	directed-message passing neural network
DoD	Department of Defense
DTE	1,5,9-decatriene
EM	energetic material
EMD	equilibrium molecular dynamics
EN	ethyl nitrate
EODT	6-ethenyl-2,8,12,16-octadecetetraene
GAFF	general AMBER force field
iPN	isopropyl nitrate
MD	molecular dynamics
ML	machine learning
MSD	mean square deviation
MYR	myrcene
NPT	constant number of particles, pressure, and temperature
PCFF	polymer-consistent force field
QM-ESM	quantum mechanical and electronic structure modeling

1 (PDF)	DEFENSE TECHNICAL INFORMATION CTR DTIC OCA
1 (PDF)	DEVCOM ARL FCDD RLB CI TECH LIB